

Robust Physical Hard-Label Attacks on Deep Learning Visual Classification

Ryan Feng¹, Jiefeng Chen², Earlence Fernandes², Somesh Jha², Atul Prakash¹

¹University of Michigan, Ann Arbor, ²University of Wisconsin, Madison

¹{rtfeng, aprakash}@umich.edu, ²{jiefeng, earlence, jha}@cs.wisc.edu

Abstract

Existing physical adversarial examples for computer vision rely on white-box access. In this work, we investigate physical examples in the *black-box hard-label* case — where the attacker has only query access to the model and only receives the top-1 class label without confidence information. This threat model is more realistic for cyber-physical systems — the main target when considering physical attacks on computer vision. Key challenges in this setting include obtaining reliability against environmental variations and creating area-limited perturbations without access to model gradients. We base our work on recent advances in gradient-free optimization and present GRAPHITE, the first algorithm for black-box hard-label physical attacks on computer vision models. We evaluate GRAPHITE on a traffic sign classifier and a publicly-available Automatic License Plate Recognition (ALPR) tool using only query access. We successfully cause a Stop sign to be misclassified as a Speed Limit 30 in 92.9% of physical test images and cause errors in 95% of cases for the ALPR tool.

1 Introduction

Machine learning (ML) models, such as deep-neural networks (DNNs), have had resounding success in several scenarios such as face and object recognition [15, 17, 33, 35, 37]. Based on this success, they are now a part of perception pipelines in cyber-physical systems (CPSs) like cars [12, 20, 27], UAVs [2, 24] and robots [40]. However, recent work has found that these models are vulnerable to attacks, such as test-time adversarial examples [5, 14, 29, 38] where an adversary subtly perturbs a benign input to cause a misclassification by the ML model.

This threat has gained recent attention and work in the computer vision community has made progress in understanding the space of adversarial examples, beginning in the digital domain and more recently, in the physical domain where attackers can perturb physical objects by plac-

ing stickers or colorful patterns [1, 4, 10, 34]. Along similar lines, our work contributes to the understanding of attacks in this space. Specifically, we investigate physical adversarial examples in the *black-box hard-label case*, where attackers only have query access to the model. That is, the attacker receives the top-1 class label without any confidence information.

We observe that this threat model more closely mirrors real-world ML deployments — many commercial or proprietary systems are closed source and only provide class labels as output. For example, the PlateRecognizer [30] Automatic License Plate Recognition (ALPR) system offers a paid service that includes a closed source vision ML model, with only API formats for prediction queries made available. Similarly, Keen Lab’s recent security analysis of auto-wipers on a Tesla shows that even with significant reverse engineering effort, it is difficult to completely reconstruct a deployed model due to proprietary formats, implementations, and stripped binaries [19], whereas, obtaining query access is much easier. Imposing hard-label access represents perhaps the weakest but most realistic threat model, as it is the minimum amount of information an ML model, including a proprietary one, has to make available for it to be useful.

The key challenge in achieving this goal is obtaining robustness to dynamic physical-world conditions (e.g., changing camera angles, distances, camera perception errors, etc.) without access to the gradients of the model. While prior work has explored this type of robustness (RP2 [10], Expectation over Transformation [1]), it depends on white-box access where small steps can be taken to find both small but robust perturbations. In the hard-label setting, we now have to optimize in an extremely flat and discontinuous output space across multiple transformations. Our key insight is to leverage recent advances in gradient-free optimization (GFO) techniques [26] and formulate a novel optimization objective that can be effectively solved using GFO while yielding robust physical examples. A related challenge lies in restricting the physical area where the perturbation can be added to the underlying object. For example, stickers of a particular shape and size on a Stop sign. We term the pro-



(a) Targeted GTSRB attack to convert a stop sign into a speed limit 30 km/hr sign, generated by GRAPHITE.

(b) Physical license plate holder sticker attack to confuse the ALPR license plate prediction. Plate was purchased online and do not refer to the authors' actual plates.

Figure 1: Example GRAPHITE attacks.

cess of generating an appropriate perturbation area as mask generation. Prior work has investigated heuristic methods to generate a suitable mask [10], but relies on white-box access and some manual experimentation to identify masks that work well.

Informed by these challenges, we contribute GRAPHITE (Gradient-free Robust Adversarial Physical Hard-label Image-based Targeted Examples), the first (to the best of our knowledge) algorithm that can generate robust physical adversarial examples for computer vision in the hard-label setting. Furthermore, as GRAPHITE is a complete attack algorithm, it also can *automatically* generate masks (i.e., perturbation position, shape and size).

We evaluate GRAPHITE along two dimensions in the physical world. First, based on prior work, we conduct an attack that generates stickers to convert a Stop sign into a Speed limit sign [10]. Using physical-world tests, we demonstrate that the perturbation, which was generated in a black-box manner using hard-label queries, is robust to viewpoint and lighting changes. Second, we create an adversarial license plate holder that could be used to evade a real-world commercial automated license plate recognition (ALPR) system for which we only have query access. These systems can be misused for mass surveillance purposes [11], and thus, our black-box hard-label attacks could serve as a mechanism to evade such surveillance and maintain privacy. Example attacks are shown in Fig. 1.

Our Contributions:

- We introduce GRAPHITE, the first physical adversarial attack in the black-box hard-label setting. We propose a novel optimization objective and provide algorithms to find robust attacks even in the discrete and discontinuous hard-label setting.
- We present, a novel mask generation process to *automatically* generate candidate masks to spatially con-

strain the perturbation.

- We demonstrate how to create an adversarial license plate holder sticker for an ALPR system, a black-box piece of software that we can only query for predictions.

2 Background and Related Work

Physical attacks on computer vision. Existing work for robust physical perturbation attacks on computer vision focuses on the white-box setting. Examples include printing images of perturbed objects [18], modifying objects with stickers [10, 34], and 3D printing perturbed objects [1]. Such attacks typically optimize the expectation over a distribution of transformations, known as *Expectation over Transformation (EOT)* [1]. In this work, we describe this quantity as the *survivability* of an attack. Additionally, some attacks introduce the notion of a mask that constrains the perturbation to small regions of the object [10].

Formally, let x be an input image, v be an appropriate norm, F be a classifier with model parameters θ , S be the perturbation space, T be a distribution over transformations, y_{adv} be the desired target label, and M_x be a mask. Such a physical attack in the white-box setting can be formulated as the following optimization problem:

$$\operatorname{argmin}_{\delta \in S} \nu(\delta) + \mathbb{E}_{t \sim T} \left[F(\theta, t(x + M_x \cdot \delta)) \neq y_{adv} \right] \quad (1)$$

All these existing methods rely on the availability of gradients from a white-box model to find perturbations that have high survivability under a range of physical transforms such as change of viewing angle, distance, and lighting. In contrast, we construct robust, physical attacks with only top-1 hard-label information, enabling us to attack real-world systems. We additionally find masks automatically, while existing work requires some manual effort to design suitable masks.

Digital black-box attacks. There are several categories of digital black-box attacks:

- **Transfer Attack:** These *transferability* techniques train a surrogate model, generate white-box examples on the surrogate, and hope they transfer to the target [28]. Unfortunately, targeted example success rates are low [22]. Additionally, many techniques require access to similar training sets that may not be available. In contrast, our work only requires query access to the target model.
- **Soft-label Attack:** These *score-based* techniques require access to the softmax layer output in addition to class labels [7, 25]. Using this information, they can

apply zeroth-order optimization or local search strategies to compute the adversarial example. In contrast, our threat model only allows the attacker top-1 predicted class label access. We construct a gradient-free optimization objective that can create robust examples using only hard-label access.

- **Hard-label Attack:** A recent line of work has started exploring hard-label attacks in the digital setting [6, 8, 9, 16], where only the top-1 label prediction is available. Such attacks are difficult because the hard-label optimization space is discontinuous and discrete. One particular algorithm of interest is OPT-attack [8], which solves this problem by reformulating the attack problem to find a perturbation direction with a minimal boundary distance.

Let x refer to a victim image that the attacker wishes the classifier F to classify as the target class y_{adv} . Thinking of the perturbation as an adversarial direction ϕ with magnitude λ , let $g(\phi)$ be the scalar distance to the nearest adversarial example in the direction ϕ , which leads to the following optimization problem:

$$\min_{\phi} g(\phi) \quad (2)$$

where:

$$g(\phi) = \min_{\lambda > 0} \lambda \text{ s.t. } \left(F \left(x + \lambda \frac{\phi}{\|\phi\|_2} \right) = y_{adv} \right) \quad (3)$$

Cheng *et al.* [8] uses the Randomized Gradient Free (RGF) method [13, 26], to optimize $g(\phi)$. The algorithm samples nearby directions and uses that to estimate a gradient. The gradient update is defined as an average of q gradient calculations \hat{g} , where

$$\hat{g} = \frac{g(\phi + \beta u) - g(\phi)}{\beta} \cdot u \quad (4)$$

In the above equation, u is a normalized, random Gaussian vector and β is a nonzero smoothing parameter. $g(\phi)$ is calculated using a binary search process. The initial perturbation direction ϕ is initialized from random example images of the target class. For more details, we refer readers to the original paper [8].

Unfortunately, direct applications of hard-label approaches like OPT-attack do not easily generate robust, physical attacks. Fundamentally, OPT-attack is designed to generate imperceptible attacks by minimizing the distance from the original image whereas physical attacks require us to maximize robustness to physical-world variance. GRAPHITE also operates in

the hard-label setting but will generate physically robust attacks, unlike existing hard-label attacks.

3 Optimization for Hard-Label Physical Attacks

In this section, we will describe optimization problems for our approach, GRAPHITE. Unlike prior work, our goal is to both find a candidate mask and the perturbation within that masked area so that the resulting image is likely to be robust when physically realized. We will first describe a joint optimization problem for finding an optimal perturbation and mask and then discuss a two-stage process that is more practical for the hard-label setting.

As in Athalye *et al.* [1], we also rely on estimating *survivability* of an image under transforms, i.e., the expectation of an image being predicted with a given label under physical world transformations (this was termed EOT in Athalye *et al.* [1]). Details on the specific transformations and ranges used are included in the supplementary material (Section A).

3.1 Problem Setup

In our approach, our goal is to find some perturbation δ and a small mask M such that when δ is applied to a victim image x our model F predicts the target label y_{adv} with high survivability. The area that δ may occupy is constrained by the mask M . The perturbations must have high expected survivability under transformations t sampled from a distribution T . To help with initialization, we will utilize an example target image x_{tar} .

3.2 Joint Optimization

With the notation above, we will first describe our new joint optimization problem. The optimal noise must maximize survivability and take up as little of the sign as possible and the pixels perturbed are identified by a mask M , where M_{ij} is 1 if pixel at position (i, j) is perturbed and 0 otherwise. These goals are in opposition and must be solved jointly to achieve the best solution ($\lambda_1 > 0$ is the relative weight given to size of the mask M in the joint optimization).

$$\operatorname{argmin}_{\delta, M} \lambda_1 \cdot \|M\|_0 - \mathbb{E}_{t \sim T} \left[F \left(t(x + M \cdot \delta) \right) = y_{adv} \right] \quad (5)$$

We argue that solving this directly is computationally challenging, especially in the hard-label setting. The first

reason is that finding an optimally-sized mask by itself is a combinatorially hard problem (we include a proof in the supplementary material (Section C) to show that it is NP-complete).

Secondly, we also operate in a very large discrete and discontinuous space when examining hard-label attacks. It is important to reformulate the problem in such a way that gradient-free methods can reasonably solve it.

Now that we have established that solving the above problem of joint optimization is both combinatorially hard (due to the notion of a mask) and difficult to characterize purely in terms of gradients, we solve a decoupled optimization problem and apply some heuristics.

3.3 Two-Step Optimization

Step #1: Mask Generation: We first find an optimized mask which when filled in with the target image x_{tar} results in at least a specified level of survivability, s_{lo} , a hyperparameter. We constrain the unmasked perturbation to be fixed at $\delta_{tar} = x_{tar} - x$ and solve the optimization objective from (5) under that constraint:

$$\begin{aligned} \operatorname{argmin}_M \quad & \lambda_1 \cdot \|M\|_0 \\ & - \mathbb{E}_{t \sim T} \left[F \left(t(x + M \cdot \delta_{tar}) \right) = y_{adv} \right] \\ \text{s.t.} \quad & \mathbb{E}_{t \sim T} \left[F \left(t(x + M \cdot \delta_{tar}) \right) = y_{adv} \right] \geq s_{lo} \end{aligned} \quad (6)$$

We show how to solve this formulation heuristically using an algorithm described in Section 4.1. Note that δ_{tar} is only applicable within the resulting mask M . (See intermediate output after Mask Generation in Figure 2).

Step #2: Boosting via Perturbation Generation: Equipped with the mask M found by the Mask Generation Optimization Problem in Step #1, we then aim to maximize survivability for the given mask by changing the perturbation δ within the masked region (see final output in Figure 2 for an example result):

$$\operatorname{argmax}_{\delta} \quad \mathbb{E}_{t \sim T} \left[F \left(t(x + M \cdot \delta) = y_{adv} \right) \right] \quad (7)$$

By using survivability as a measure of physical robustness, we can leverage this function as an optimization goal we can pursue even in the hard-label case (described in Section 4.2). In the supplementary material (Section B.0.3), we provide empirical evidence to suggest that this function has relatively low Lipschitz constants even when approximating the expectation in (7) by averaging over n transformations. We additionally refer to this process as *boosting* the

survivability, as we start with a perturbation δ with lower survivability and attempt to boost it as high as we can.

4 Generating Hard-Label Physical Attacks with GRAPHITE

We now describe how to solve the mask and perturbation generation problems presented in Section 3 in the hard-label setting. For ease of algorithmic notation, given a mask M and perturbation δ the survivability in (7) can be estimated as follows by computing n randomly sampled transformations $t_i \sim T$:

$$S(M, \delta) = \frac{\sum_{i=1}^n \mathbb{1} \left[F \left(t_i(x + M \cdot \delta) \right) = y_{adv} \right]}{n} \quad (8)$$

Fig. 2 shows the algorithm flow along with intermediate and final results. The figure covers the mask generation and boosting phases we will discuss next.

4.1 Mask Generation

We need to find a candidate mask that has good initial survivability and small size. Boosting (described in 4.2) can take care of further improving the survivability.

An example output and algorithm flow for the mask generation phase is in Fig. 2. The resulting image after this phase consists of the target image inside of the mask M and the victim image everywhere else. Or in other words, the resulting image at this stage is $x + M \cdot (x_{tar} - x)$.

We generate masks using a three stage process:

1. Heatmap Estimation
2. Coarse-grained Mask Reduction
3. Fine-grained Mask Reduction

We initialize the mask to cover the entire victim object with the target object. We then choose a group of pixels called a *patch* as a configurable input into the algorithm. The patch serves two purposes: (1) it helps us estimate a heatmap (i.e., which regions of pixels contribute more to survivability) and (2) it is used to remove groups of pixels from the mask to reduce the size of the mask as the algorithm optimizes the mask objective function (6).

4.1.1 Heatmap Estimation

We first generate a ‘‘heatmap’’ (similar to a saliency map) over the image by estimating the impact of removing one patch at a time at each possible pixel position in the initial mask and then measuring the resulting target’s survivability. If the survivability remains high after patch removal, those

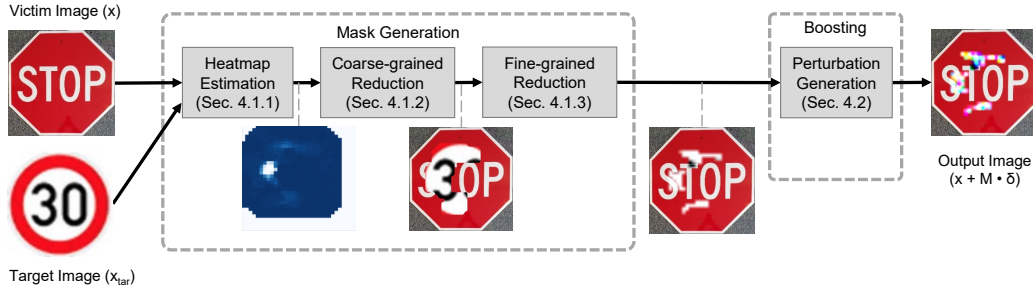


Figure 2: Figure showing the algorithm flow with intermediate and final results for a targeted attack on a Stop sign to Speed limit 30 km / hr sign.

pixels are likely unimportant to causing a target prediction. By contrast, the more the survivability drops, the more important the patch area is to causing a target prediction. This process enables us to identify candidate regions to remove from the mask. We refer to the drop in survivability from removal of a patch as the *impact* of that patch.

We note that it is critical to pick a reasonable patch size because of the hard-label restriction. In one extreme, if we pick a single pixel as our patch, we are extremely unlikely to get any useful survivability signal because the survivability will likely be the same with or without that single pixel. If we make the patch too large, we lose the ability to make more general mask shapes and could remove too much at a time from the mask. In our experiments, for 32×32 images, we empirically found that a 4×4 square patch worked well. Example heatmaps and discussion points are included in the supplementary material (Section E).

4.1.2 Coarse-grained Mask Reduction

Utilizing the information in the heatmap, we want to begin reducing the size of the mask. As an optimization to save queries, we do a coarse-grained pruning initially. We posit that if we sort the patches from least impactful to most impactful, the order will be highly reflective of the probability of inclusion of these patches in the final mask. Thus, we initially sort and perform a fast reduction of our mask through binary search. Specifically, we find the point *pivot* in the ordered queue of patches \mathcal{P} such that the bitwise unions of patches from that point ($\bigcup_{i=pivot}^{|\mathcal{P}|} \mathcal{P}_i$) yields a mask of survivability $\geq s_{hi}$, where s_{hi} is a hyper-parameter specifying a high survivability threshold that must be reached. If s_{hi} cannot be reached, we simply include all patches. Compared to starting with the full object covering mask and reducing patches one by one, this initialization process allows us to cut out the low impact patches faster. A comparison with and without coarse reduction is included in the supplementary material (Section E).

4.1.3 Fine-grained Mask Reduction

We then execute a fine-grained reduction that uses a greedy algorithm to improve the objective score of (6). The algorithm starts from low impact patches (i.e, low impact on target survivability) to high impact patches and greedily removes patches if it improves the objective function. Conceptually, this objective function is designed to reward smaller masks and penalize low survivability. Algorithmically, we found the attack to be more effective if we additionally added a restriction that survivability does not cross below some minimum threshold, s_{lo} .

Let n be the number of transforms and \mathcal{P} be the set of valid patches. The number of queries is then bounded by $O(n \cdot |\mathcal{P}|)$. In the worst case, we make two full passes over each patch (once for heatmap estimation and once in reduction), plus at most $\log |\mathcal{P}|$ queries for a binary search.

4.2 Perturbation Generation (Boosting)

Given a resulting image x and a mask M from the previous stage, survivability boosting, or simply *boosting*, aims to find the perturbation δ to add to x to create a targeted adversarial example for class y_{adv} that can survive physical-world transformations with the highest probability (see Equation 7). By directly optimizing over *survivability* with respect to the target label, we aim to create robust physical attacks that are constrained to a perturbation space defined by the mask M . Survivability also gives us a function whose gradient we can estimate. We use the Randomized Gradient-Free (RGF) method [13, 26] to find maximally robust perturbations.

Our perturbation generation process has several crucial differences from OPT-style attacks [8]. The first is that we have a survivability based re-formulation instead of a distance based re-formulation. We use the initial target example x_{tar} to initialize the perturbation within the mask bounds and then begin maximizing survivability. By contrast, OPT-attack interpolates between victim and target images to find the boundary, and then effectively searches near

the boundary to find closer points to the victim. This process requires frequent calculations of the boundary distance, which they calculate with query-intensive binary search operations. We do not need to continually locate the boundary because we optimize over a survivability metric that we can compute directly over n transformation samples.

Once the perturbation δ has been initialized $M \cdot (x_{tar} - x)$, we proceed to maximize the probability that a perturbation will remain robust to physical-world transforms with the RGF [13, 26] method for gradient estimation using q random samples for each gradient estimation. Explicitly, let u be random Gaussian unit vectors within the allowable range of the mask. Then, the gradient update is as follows:

$$\hat{g} = \frac{S(M, \delta + \beta u) - S(M, \delta)}{\beta} \cdot u \quad (9)$$

Finally, we introduce the notion of a query budget which limits the amount of queries used in a particular stage of the algorithm. These parameters can be tuned to emphasize better mask generation or better boosting without a budget of queries if we want to limit the number of attack queries.

4.3 Theoretical Analysis

GRAPHITE has two main sources of error that can affect perturbation quality: (a) Sampling error: we sample a set of transformations to estimate a solution to Equation (7) and (b) GFO error: in the hard-label setting, we do not have access to gradient information. In the supplementary material (Section B), we discuss sampling error bounds, show that GFO error and efficiency is proportional to the Lipschitz constant of the objective function, and that empirically our objective has a low Lipschitz constant (≤ 0.0537).

5 Experiments

We demonstrate the viability of GRAPHITE by attacking a traffic sign classifier trained on German Traffic Sign Recognition Benchmark (GTSRB) [36] data and by attacking a real-world ALPR system. We show that our results are robust to physical world transforms. We do this by both reporting *digital survivability* results on a broader range of attacks and a subset of *physical survivability* results to confirm that our digitally robust examples translate to the physical world in the form of stickers.

5.1 Experimental Setup

Datasets and Classifiers. We use the classifier from RP2 [10, 39] trained on an augmented GTSRB dataset [36]. As with RP2 [10], we replace the German Stop signs with U.S. Stop signs from the LISA dataset [23]. As a validation

Table 1: Sample of digital targeted attacks on GTSRB-Net. Ran with $s_{lo} = 70\%$, $s_{hi} = 90\%$, $n = 100$ during attack. Final survivability calculated on $n = 1000$ transformations.

Victim	Target	Final Surv.	Mask to Object Ratio
Stop	SL20	79%	4.99%
Stop	Ped. Crossing	78.7%	10.68%
Stop	Turn Left	84.3%	7.83%
Stop	SL30	90%	9.97%
SL30	SL20	98.1%	2.26%
SL30	Ped. Crossing	95.4%	21.54%
SL30	Turn Left	97.1%	9.49%

Table 2: Lab results of targeted attack (Stop sign to speed limit 30 km / hr) on GTSRB-Net under different angles and distances compared against a baseline of clean Stop signs. 5 pictures taken at each angle / distance pair listed at mid-day and 5 pictures taken at each angle / distance pair at evening.

Distance / Angle	SL 30 Success (%)	Avg. SL 30 Conf. on Successes
5' 0°	100%	0.993335
5' 15°	100%	0.976236
5' 30°	100%	0.946215
5' 45°	100%	0.45445
10' 0°	100%	0.997888
10' 15°	100%	0.898794
10' 30°	90%	0.885375
15' 0°	90%	0.861517
15' 15°	80%	0.800151
20' 0°	80%	0.8663294
20' 15°	100%	0.892987
25' 0°	90%	0.854974
30' 0°	90%	0.946917
40' 0°	80%	0.777677
Aggregate (day)	94.29%	0.853619
Aggregate (evening)	91.43%	0.886951
Aggregate (total)	92.86%	0.870285

set, we take out the last 10% from each class in the training set. We also augment the dataset with random rotation, translation, and shear, following Eykholt *et al.* [10]. Our network, GTSRB-Net, has a 97.656% test set accuracy.

In both attacks, we use our own victim image of the source object and use an Internet image outside of the

dataset for initialization to demonstrate that GRAPHITE does not rely on having training set images to initialize from. In our experiments we assume that object boundaries are available, but note they could be obtained automatically through an object segmentation network [32].

For ALPR, we use OpenALPR version 2.3.0, the latest freely available version. We treat the provided command line tool as a complete black-box. (Note that while this particular tool provides confidence info, others may not. Thus, we throw away any confidence info during our attack). For the initialization image, we use the same image but with a gray rectangle filled in with (127, 127, 127) at each pixel over the license plate.

More details about hyper-parameters are included in the supplementary material (Section D).

GTSRB Attack Details. We set the size of our input images to be 244×244 and used 100 randomly chosen transformations in the attack. During the attack, we first generate 32×32 perturbations and then upsample to the resolution of the input image whenever they have to be added together.

We classify our objects at stationary positions to test how robust our attacks are to different viewing conditions. To examine robustness against geometric changes, we take five pictures of the perturbed stop sign at 14 different locations for a total of 70 pictures. To compare against baseline Stop sign accuracy, we also take five pictures of a clean Stop sign at each of the same 14 locations. The 14 locations were chosen based on RP2 evaluation [10]. To test lighting conditions, we take one set of images in sunny mid-day conditions and one in the evening with less direct sunlight.

To gather crops we use the original author’s YOLOv3 [31] object detector network trained on MS COCO [21] to predict bounding boxes for the stop sign. We take the output bounding boxes, crop the sign accordingly, resize to 32×32 , and send to our network for classification.

We generated an example attack that took approximately 9 mins with a boost budget of 20k queries. In total with mask generation, it used 123.7k queries. It modeled 100 transformations and digitally survived 93% of those transformations. When confirming survivability on 1000 transformations, the attack survived 90% of transformations.

ALPR Attack Details. To attack ALPR systems, we imagine printing a license plate holder sticker to cause the ALPR system to fail to detect your license plate number correctly. In this case, we are given a known mask, and could attack with just the boosting stage. However, starting from just this point may lead to poor initial survivability, so we now describe how to use multiple rounds of mask generation and boosting to combat this.

To initialize the border noise, we can fix the border as part of the mask and then start minimizing the inner noise

Table 3: Sample of lab-test images of targeted attack (stop sign to speed limit 30 km / hr) on GTSRB-Net.

Dist. / Angle	Image	Dist. / Angle	Image
5' 0°		10' 15°	
5' 15°		10' 30°	
5' 30°		15' 0°	
5' 45°		15' 15°	
10' 0°		20' 0°	

by alternating mask generation and boosting. Over time, the perturbation becomes less reliant on inner noise and more so on just the noise in the border. Then, we can set the mask to just the border and run a final perturbation boosting stage.

To test our ALPR attack, we print out the license plate holder stickers and place it on a car and an outdated license plate. Note that the license plate was purchased online and does not refer to the authors’ actual plates. We ran ALPR on stationary pictures of the car taken in an empty parking lot and took five pictures of the car at 5’, 10’, 15’, and 20’ away at both 0 and 15 degree angles. We generate our attack on a 724×500 size image. The perturbation was generated at 362×250 and enlarged to fit over the whole image.

As with GTSRB, we use the original author’s YOLOv3 [31] object detector network trained on MS COCO [21] to predict bounding boxes for the car. We take the output bounding boxes, crop the sign accordingly, resize the crops such that the height is 500 pixels, and send the crops to the black-box ALPR pipeline.

We set the target to be that the ALPR fails to detect any license plates. We used 3 iterations of mask generation and boosting. The patch size for mask generation was 8×8 , then 4×4 , and then in the last iteration the mask was fixed to just the border. The stride for the patches was the width divided by 2. We additionally added in the backtracking line search

Table 4: Sample of lab-test images of targeted ALPR attack, cropped and zoomed into the license plate to show the perturbation better. Plate was purchased online and do not refer to the authors’ actual plates.

Dist. / Angle	Image	Dist. / Angle	Image
5’ 0°		15’ 0°	
5’ 15°		15’ 15°	
10’ 0°		20’ 0°	
10’ 15°		20’ 15°	

to adaptively select the step size as in OPT-attack [8]. The attack took 8115 queries and generated a result with 85.7% digital survivability rate over 1000 transformations.

5.2 Experimental Results

Digital Survivability Tests. We report a subset of results when run with a high threshold $s_{hi} = 90\%$ for coarse-grained mask reduction and a low threshold $s_{lo} = 70\%$ for fine-grained mask reduction. We note that a higher s_{hi} helps ensure that the coarse-grained reducer does not remove useful patches while a higher s_{lo} increases the odds that the final boosted survivability is higher, as it provides a better starting point after mask generation. We note that these parameters can be tuned based on the specific victim target pairs and to tradeoff more subtle noise and survivability.

In this section, we generate attacks with $n = 100$ transformations during the attack and then calculate the final survivability on $n = 1000$ transformations. A sample of results are shown in Table 1. We show that we can attack with a variety of victim and target pairs and achieve greater than 75% survivability, with often 10% or less of the original object perturbed. Images of these attacks are included in the supplementary material (Section E).

Physical Robustness Lab Tests. We also carried out physical object perturbation experiments in the field to confirm physical survivability. In the next sections, we evaluate GRAPHITE on a targeted attack with a victim image

of a stop sign with a target label of speed limit 30 km/hr at different viewing angles and lighting conditions. We also evaluate an ALPR license plate holder attack.

- **GTSRB Results:** Table 2 shows the results of the lab tests for our test perturbation, and Table 3 shows a subset of images used in the test. We include the percentage of images labeled as speed limit 30 km/hr and the average speed limit 30 km/hr confidence on successes.

Overall, 92.86% of the 140 total images (one set of five at each location mid-day and another set in the evening) were classified as speed limit 30 km/hr. There was not too much variation across either lighting changes or geometric changes, with all spots yielding a successful attack image at least 80% of the time and with little difference between mid-day and evening photos (94.29% vs 91.43%). These results suggest that our perturbations are robust to environmental changes captured by viewing perspectives and lighting. The average confidence is above 85% as well. We also confirmed that the speed limit 30 km/hr classifications were due to our stickers with a separate baseline test suite on a clean Stop sign. In the baseline, all 100% of the clean Stop sign images were correctly classified.

- **ALPR Results:** Table 4 shows example crops from our ALPR experiments. We found that 95% of the 40 images caused an error in the license plate detection. 40% of the images caused the ALPR system to fail to detect any plates and 55% of the images caused the ALPR system to incorrectly predict the license plate. Of the incorrect guesses, the average Levenshtein distance, which calculates the number of additions, subtractions, and substitutions required to change one string to another, was 3.04545. We include a per spot breakdown in Table 5. 100% of unperturbed, baseline images correctly predicted the license plate.

6 Conclusion

We developed GRAPHITE, first algorithm for hard-label physical attacks on classification networks. GRAPHITE addresses limitations in existing physical attacks to work in the discrete and discontinuous hard-label setting, which is the most realistic threat model for cyber-physical systems. By formulating a novel optimization objective that can be solved with gradient-free optimization, we are able to develop physically robust perturbations without model gradients. We demonstrate feasible perturbations for attacking a traffic sign classifier and an automated license plate recognition (ALPR) system, bridging the gap to being able to attack real-world models in the hard-label setting.

Table 5: ALPR results. 5 pictures taken at each angle / distance pair.

	5' 0°	10' 0°	15' 0°	20' 0°	5' 15°	10' 15°	15' 15°	20' 15°
No Plates Detected	40%	20%	80%	40%	20%	20%	40%	60%
Misreads	40%	80%	20%	60%	80%	60%	60%	40%
Correct	20%	0%	0%	0%	0%	20%	0%	0%
Lev. Dist of Misreads	2	3.75	1	4.33	3.25	3	3	1.5

Acknowledgement

This material is based on work supported by DARPA under agreement number 885000, Air Force Grant FA9550-18-1-0166, the National Science Foundation (NSF) Grants 1646392, CCF-FMitF-1836978, SaTC-Frontiers-1804648 and CCF-1652140, and ARO grant number W911NF-17-1-0405. Earlene Fernandes is supported by the University of Wisconsin-Madison Office of the Vice Chancellor for Research and Graduate Education with funding from the Wisconsin Alumni Research Foundation. The U.S. Government is authorized to reproduce and distribute reprints for Governmental purposes notwithstanding any copyright notation thereon. Any opinions, findings, and conclusions or recommendations expressed in this material are those of the author(s) and do not necessarily reflect the views of our research sponsors.

References

- [1] Anish Athalye, Logan Engstrom, Andrew Ilyas, and Kevin Kwok. Synthesizing robust adversarial examples. *arXiv preprint arXiv:1707.07397*, 2017. [1](#), [2](#), [3](#), [10](#)
- [2] Haitham Bou-Ammar, Holger Voos, and Wolfgang Ertel. Controller design for quadrotor uavs using reinforcement learning. In *Control Applications (CCA), 2010 IEEE International Conference on*, pages 2130–2135. IEEE, 2010. [1](#)
- [3] Stéphane Boucheron, Gábor Lugosi, and Pascal Massart. *Concentration Inequalities*. Oxford University Press, 2013. [12](#)
- [4] Tom B. Brown, Dandelion Mané, Aurko Roy, Martín Abadi, and Justin Gilmer. Adversarial patch. *arXiv preprint arXiv:1712.09665*, 2017. [1](#)
- [5] Nicholas Carlini and David Wagner. Towards evaluating the robustness of neural networks. In *2017 IEEE Symposium on Security and Privacy (SP)*, pages 39–57. IEEE, 2017. [1](#)
- [6] Jianbo Chen, Michael I Jordan, and Martin J Wainwright. Hopskipjumpattack: A query-efficient decision-based attack. *arXiv preprint arXiv:1904.02144*, 2019. [3](#)
- [7] Pin-Yu Chen, Huan Zhang, Yash Sharma, Jinfeng Yi, and Cho-Jui Hsieh. Zoo: Zeroth order optimization based black-box attacks to deep neural networks without training substitute models. In *Proceedings of the 10th ACM Workshop on Artificial Intelligence and Security*, pages 15–26. ACM, 2017. [2](#)
- [8] Minhao Cheng, Thong Le, Pin-Yu Chen, Jinfeng Yi, Huan Zhang, and Cho-Jui Hsieh. Query-efficient hard-label black-box attack: An optimization-based approach. In *International Conference on Learning Representations*, 2019. [3](#), [5](#), [8](#)
- [9] Minhao Cheng, Simranjit Singh, Pin-Yu Chen, Sijia Liu, and Cho-Jui Hsieh. Sign-opt: A query-efficient hard-label adversarial attack. *arXiv preprint arXiv:1909.10773*, 2019. [3](#)
- [10] Kevin Eykholt, Ivan Evtimov, Earlene Fernandes, Bo Li, Amir Rahmati, Chaowei Xiao, Atul Prakash, Tadayoshi Kohno, and Dawn Song. Robust Physical-World Attacks on Deep Learning Visual Classification. In *Computer Vision and Pattern Recognition (CVPR)*, June 2018. [1](#), [2](#), [6](#), [7](#), [10](#)
- [11] Electronic Frontier Foundation. Street-Level Surveillance: Automated License Plate Readers (ALPRs). <https://www.eff.org/pages/automated-license-plate-readers-alpr>. [2](#)
- [12] Andreas Geiger, Philip Lenz, and Raquel Urtasun. Are we ready for autonomous driving? the kitti vision benchmark suite. In *Computer Vision and Pattern Recognition (CVPR), 2012 IEEE Conference on*, pages 3354–3361. IEEE, 2012. [1](#)
- [13] Saeed Ghadimi and Guanghui Lan. Stochastic first-and zeroth-order methods for nonconvex stochastic programming. *SIAM Journal on Optimization*, 23(4):2341–2368, 2013. [3](#), [5](#), [6](#)
- [14] Ian J Goodfellow, Jonathon Shlens, and Christian Szegedy. Explaining and harnessing adversarial examples. *arXiv preprint arXiv:1412.6572*, 2014. [1](#)
- [15] Kaiming He, Xiangyu Zhang, Shaoqing Ren, and Jian Sun. Deep residual learning for image recognition. In *Proceedings of the IEEE conference on computer vision and pattern recognition*, pages 770–778, 2016. [1](#)
- [16] Andrew Ilyas, Logan Engstrom, Anish Athalye, and Jessy Lin. Black-box adversarial attacks with limited queries and information. In *Proceedings of the 35th International Conference on Machine Learning*, pages 2137–2146, 2018. [3](#)
- [17] Alex Krizhevsky, Ilya Sutskever, and Geoffrey E Hinton. Imagenet classification with deep convolutional neural networks. In *Advances in neural information processing systems*, pages 1097–1105, 2012. [1](#)
- [18] Alexey Kurakin, Ian Goodfellow, and Samy Bengio. Adversarial examples in the physical world. *arXiv preprint arXiv:1607.02533*, 2016. [2](#)
- [19] Tencent Keen Security Lab. Experimental Security Analysis of Tesla AutoPilot. <https://keenlab.tencent.com/en/whitepapers/>

[Experimental_Security_Research_of_Tesla_Autopilot.pdf](#). 1

- [20] Timothy P Lillicrap, Jonathan J Hunt, Alexander Pritzel, Nicolas Heess, Tom Erez, Yuval Tassa, David Silver, and Daan Wierstra. Continuous control with deep reinforcement learning. *arXiv preprint arXiv:1509.02971*, 2015. 1
- [21] Tsung-Yi Lin, Michael Maire, Serge Belongie, James Hays, Pietro Perona, Deva Ramanan, Piotr Dollár, and C Lawrence Zitnick. Microsoft coco: Common objects in context. In *European conference on computer vision*, pages 740–755. Springer, 2014. 7
- [22] Yanpei Liu, Xinyun Chen, Chang Liu, and Dawn Song. Delving into transferable adversarial examples and black-box attacks. *CoRR*, abs/1611.02770, 2016. 2
- [23] Andreas Mogelmoose, Mohan Manubhai Trivedi, and Thomas B Moeslund. Vision-based traffic sign detection and analysis for intelligent driver assistance systems: Perspectives and survey. *IEEE Transactions on Intelligent Transportation Systems*, 13(4):1484–1497, 2012. 6
- [24] Christian Mostegel, Markus Rumpfer, Friedrich Fraundorfer, and Horst Bischof. Uav-based autonomous image acquisition with multi-view stereo quality assurance by confidence prediction. In *Proceedings of the IEEE Conference on Computer Vision and Pattern Recognition Workshops*, pages 1–10, 2016. 1
- [25] Nina Narodytska and Shiva Kasiviswanathan. Simple black-box adversarial attacks on deep neural networks. In *2017 IEEE Conference on Computer Vision and Pattern Recognition Workshops (CVPRW)*, pages 1310–1318, July 2017. 2
- [26] Yurii Nesterov and Vladimir Spokoiny. Random gradient-free minimization of convex functions. *Foundations of Computational Mathematics*, 17(2):527–566, 2017. 1, 3, 5, 6, 12
- [27] OpenPilot. OpenPilot on the Comma Two. <https://github.com/commaai/openpilot>, 2020. 1
- [28] Nicolas Papernot, Patrick McDaniel, and Ian Goodfellow. Transferability in machine learning: from phenomena to black-box attacks using adversarial samples. *arXiv preprint arXiv:1605.07277*, 2016. 2
- [29] Nicolas Papernot, Patrick McDaniel, Somesh Jha, Matt Fredrikson, Z Berkay Celik, and Ananthram Swami. The limitations of deep learning in adversarial settings. In *2016 IEEE European symposium on security and privacy (EuroS&P)*, pages 372–387. IEEE, 2016. 1
- [30] Plate Recognizer. Plate Recognizer Automatic License Plate Recognition Software. <https://platerrecognizer.com/>. 1
- [31] Joseph Redmon and Ali Farhadi. Yolov3: An incremental improvement. *arXiv preprint arXiv:1804.02767*, 2018. 7
- [32] Olaf Ronneberger, Philipp Fischer, and Thomas Brox. U-net: Convolutional networks for biomedical image segmentation. In *International Conference on Medical image computing and computer-assisted intervention*, pages 234–241. Springer, 2015. 7
- [33] Florian Schroff, Dmitry Kalenichenko, and James Philbin. Facenet: A unified embedding for face recognition and clustering. In *Proceedings of the IEEE conference on computer vision and pattern recognition*, pages 815–823, 2015. 1
- [34] Mahmood Sharif, Sruti Bhagavatula, Lujo Bauer, and Michael K. Reiter. Accessorize to a crime: Real and stealthy attacks on state-of-the-art face recognition. In *Proceedings of the 2016 ACM SIGSAC Conference on Computer and Communications Security, CCS '16*, page 1528–1540, 2016. 1, 2
- [35] Karen Simonyan and Andrew Zisserman. Very deep convolutional networks for large-scale image recognition. *arXiv preprint arXiv:1409.1556*, 2014. 1
- [36] Johannes Stallkamp, Marc Schlipsing, Jan Salmen, and Christian Igel. Man vs. computer: Benchmarking machine learning algorithms for traffic sign recognition. *Neural networks*, 32:323–332, 2012. 6, 13
- [37] Christian Szegedy, Vincent Vanhoucke, Sergey Ioffe, Jon Shlens, and Zbigniew Wojna. Rethinking the inception architecture for computer vision. In *Proceedings of the IEEE conference on computer vision and pattern recognition*, pages 2818–2826, 2016. 1
- [38] Christian Szegedy, Wojciech Zaremba, Ilya Sutskever, Joan Bruna, Dumitru Erhan, Ian Goodfellow, and Rob Fergus. Intriguing properties of neural networks. *arXiv preprint arXiv:1312.6199*, 2013. 1
- [39] Vivek Yadav. p2-traffic signs. <https://github.com/vxy10/p2-TrafficSigns>, 2016. 6
- [40] Fangyi Zhang, Jürgen Leitner, Michael Milford, Ben Upcroft, and Peter Corke. Towards vision-based deep reinforcement learning for robotic motion control. *arXiv preprint arXiv:1511.03791*, 2015. 1

Appendices

We include additional experimental and theoretical material in these appendices. In Section A we discuss further details about our physical transformations. In Sections B and C we discuss theoretical findings on GFO and mask generation. Section D discusses hyperparameter details, Section E provides additional experimental results, and Section F includes further discussion and limitations.

A Modeling Physical Transforms using Classical Computer Vision

Prior work by Eykholt et al. [10] and Athalye et al. [1] model environmental effects to create physical-world attacks in the white-box setting. These transformations account for varying conditions such as the distance and angle of the camera, lighting conditions, etc. Based on this work, we build a more principled set of transformations using classical computer vision techniques. To this end, we group these effects into 3 main classes of transformations:

1. **Geometric transformations:** These transformations refer to shape-based changes including rotation, translation and zoom. For planar objects, all three effects

can be captured in a single perspective transformation through a homography matrix. Homography matrices relate two planar views under different perspectives.

Geometrically, to convert points from one image plane to another, one can break down the operation into a rotation and translation matrix R , perspective projection onto a plane (P), and an affine transformation from plane to pixels (A). In the planar case, this boils down to a 3×3 homography matrix H :

$$x_{out} = APRx_{in} = Hx_{in} \quad (10)$$

We use these homographies to simulate rotation around the y axis and different viewing distances for given ranges of values. Once we pick values for each of the parameters uniformly, we construct the homography matrix to compute the transformation.

After performing the perspective transform, we random crop to the tightest square crop that includes the whole object $\pm c\%$ of the resultant image size to adjust for cropping errors. We also add random offsets for the crop, given as two more parameters. Then, we resize the square to the original resolution.

2. **Radiometric transformations:** These are appearance-based transformations with effects such as lighting-based changes. One technique to perform brightness adjustments is gamma correction, which applies a nonlinear function. Separately, printers apply nonlinear functions to their colorspace as well. Gamma correction is reflective of nonlinear human sight perception. To model these radiometric-based changes, we model gamma correction under gamma values between $\frac{1}{\gamma}$ and γ , with half coming from $[\frac{1}{\gamma}, 1]$ and half coming from $[1, \gamma]$ in expectation where γ is the maximum gamma value allowed. Assuming the image ranges from $[0, 1]$, this is defined as the following:

$$x_{out} = x_{in}^{\gamma} \quad (11)$$

3. **Filtering transformations:** These transformations model changes related to the camera focus. We model Gaussian blurring of different kernel sizes to measure the effects of the target object being out-of-focus. We note that as a side benefit, this may help deal with printer error as some precision in color values is lost in printing.

We define a single transformation to be a composite function that includes one of each type of modeled transformation. In our case with those listed above, we would



Figure 3: Examples of different transformed images. The upper-left image is the original, and the rest are three examples of transformed versions with perspective, lighting, and blurring transforms.

have a perspective transform followed by a cropping operation, gamma correction, and a Gaussian blur convolution. Examples of transformed images are shown in Figure 3.

B Theoretical Analysis

GRAPHITE has two main sources of error that can affect the perturbation quality: (a) Sampling error: we sample a set of transformations to estimate a solution to Equation (7) and (b) GFO error: in the hard label setting, the attacker does not have access to gradient information. GRAPHITE uses gradient-free optimization that samples a range of random Gaussian vectors leading to errors in gradient estimation. In this section, we provide an analysis of these two errors. We first show that solving the approximation approaches the true solution given enough sampled transformations implying that sampling introduces a very low error in the optimum with high probability. Second, for a fixed error in perturbation value, the number of boosting iterations (Sec. 4.2) that GRAPHITE needs is proportional to the Lipschitz constant of the objective function. Section B.0.3 contains experimental results showing that our objective has a low Lipschitz constant without big jumps.

B.0.1 Sampling Error Bounds

Let δ_1 be the solution to (7) and δ_2 be the solution to version estimated over n samples. Then we have the following:

With probability at least $1 - 2e^{-\frac{n\epsilon^2}{3}}$ we have that $|G(\delta_1) - G'(\delta_2)| < \epsilon$, where G and G' is the function being optimized in (7) and a version of (7) approximated with n transforms respectively.

With the requisite choice of n and ϵ we can make the probability $1 - 2e^{-\frac{npq^3}{3\epsilon^2}}$ very close to one. Intuitively, it means that *with high probability sampling introduces a very small error in the value of the optimum*. A proof of this statement follows.

There are several versions of Chernoff's bounds [3]. We state in Theorem 1 a form that is most convenient for us.

Theorem 1 Let X_1, \dots, X_n be iid binary variables such that $P(X_i = 1) = p$ (thus $P(X_i = 0) = 1 - p$), and let $A = \sum_{i=1}^n X_i$. In this case, we have the following inequality:

$$P\left(\left|\frac{A}{n} - p\right| \geq \zeta p\right) \leq 2e^{-\frac{np\zeta^2}{3}} \quad (12)$$

Consider the probability inside (7), which we denote as q . Let us sample n transformations $\{t_1, \dots, t_n\}$ from distribution T . Let X_i be equal to 1 if $F(t(x + M \cdot \delta)) \neq y_{adv}$, and 0 otherwise. By definition $P(X_i = 1)$ is equal to q . By Theorem 1 we have that (we instantiate the theorem with $\epsilon = \zeta q$ and $A = \sum_{i=1}^n X_i$), where ϵ represents the error in our solution due to sampling.

$$P\left(\left|\frac{A}{n} - q\right| \geq \epsilon\right) \leq 2e^{-\frac{npq^3}{3\epsilon^2}} \quad (13)$$

Or in other words

$$P\left(\left|\frac{A}{n} - q\right| < \epsilon\right) \geq 1 - 2e^{-\frac{npq^3}{3\epsilon^2}} \quad (14)$$

B.0.2 GFO Error

We give some background on *gradient-free optimization (GFO)*. For details we refer to [26]. Let $f : E \rightarrow \mathbb{R}$ be a function, where $E = \mathbb{R}^n$. Define its Gaussian approximation $f_\mu(x)$ as follows:

$$f_\mu(x) = \int_E f(x + \mu u) p_N(u) du \quad (15)$$

Where $p_N(u)$ is the probability-density function (pdf) a n -dimensional multi-variate Gaussian $\mathcal{N}(0, \Sigma)$. In GFO, one replaces the gradient of f in the descent procedure to find the optimum of $g_\mu(x)$ as follows: pick u distributed according $\mathcal{N}(0, \Sigma)$ and define it as:

$$\frac{f(x + \mu u) - f(x)}{\mu} \cdot \Sigma^{-1} \cdot u \quad (16)$$

In other words we take a directional derivative in the direction of a random Gaussian. Note that the derivative can be evaluated by black-box queries on f . Further note that the function we are optimizing is not convex and also might not be differentiable, so we are in the second case of [26, Section 7]. Essentially the number of iterations needed to achieve a certain error is proportional to the Lipschitz constant of the function f .

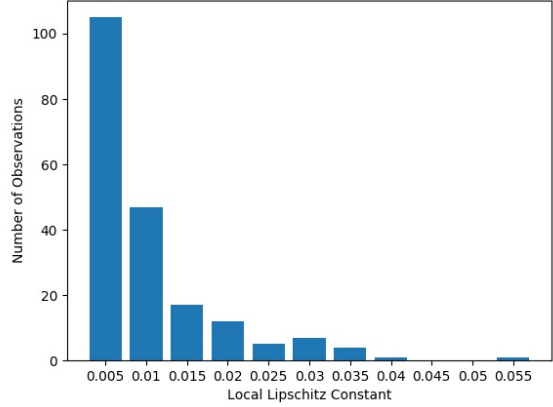


Figure 4: This figure shows a histogram of our approximate local Lipschitz constant observations on survivability. The constants are binned in intervals of 0.005 with the label being the right side of the interval. This graph shows that survivability does not vary too much per amount of change.

B.0.3 Lipschitz constants

To demonstrate that our object has a low local Lipschitz constant, we execute boosting on an example stop sign to speed limit 30 km/hr attack with $n = 1000$ transformations and approximate the local Lipschitz constant every time we compute $S(M, \delta + \beta \cdot u)$. The approximate local Lipschitz constant is given by $\frac{|S(M, \delta + \beta \cdot u) - S(\delta)|}{|\beta \cdot u|}$. We found that the maximum observed local Lipschitz constant was 0.0537. We include a histogram of observed local Lipschitz constants in Fig. 4. From Fig. 4, we can see the majority of these values are very low. From the previous section it is clear that low local Lipschitz constants lead to better convergence.

C NP-Completeness of Mask Generation

A $n \times n$ square grid is represented as G_n , which is a graph (V_n, E_n) (V_n has vertices (i, j) , where $0 \leq i \leq n$ and $0 \leq j \leq n$ and for each (i, j) , $\{(i, j + 1), (i, j - 1), (i + 1, j), (i - 1, j)\} \cap V_n$ is in the set of edges E_n). A *mask* M is a sub-graph of the grid G_n that corresponds to a contiguous region of squares. Let $C(G_n)$ be the set of masks corresponding to the grid G_n . Let $\mu : C(G_n) \rightarrow \mathbb{R}^+$ be a *monotonic scoring function* ($M \subseteq M'$ implies that $\mu(M) \leq \mu(M')$). The mask generation problem can be stated as follows: Given r and threshold t , find a mask M of size $\leq r$ (the size of the mask is number of squares in it) such that $\mu(M) \geq t$. We call this problem $\text{MASK}_P(n, \mu, r, t)$.

Simply enumerating masks is not feasible because the number of masks could be exponential. We provide a sim-

ple argument. Consider a $k \times k$ sub-grid of G_n . Consider columns that are odd numbered (i.e. of the form (i, \star) , where i is odd). Now any choice of one square for the even columns gives us a contiguous mask, so there are $\geq 2^{\frac{k(k+1)}{2}}$ masks. There are $(n - k)^2 k \times k$ sub-grids in G_n . So a lower bound on masks of size k is at least $(n - k)^2 2^{\frac{k(k+1)}{2}}$. Next we prove that our problem is actually NP-complete.

The Set Cover. Given a universe \mathcal{U} and a family \mathcal{S} of subsets of \mathcal{U} , a cover is a subfamily $\mathcal{C} \subseteq \mathcal{P}(\mathcal{U})$ of sets whose union is \mathcal{U} . In the set-covering decision problem, the input is a triple $(\mathcal{U}, \mathcal{S}, k)$ (k is an integer), and the question is whether there is a set covering of size k or less. In the set covering optimization problem, the input is a pair $(\mathcal{U}, \mathcal{S})$ and the task is to find a set covering that uses the fewest sets. The set-covering decision problem is known to be NP-complete.

Theorem 1 *Problem $MASK_P$ is NP-complete.*

Proof. Our reduction will be from the decision set-cover problem. Assume we are given an instance of the set-cover problem $(\mathcal{U}, \mathcal{S}, k)$. Let $n = \max(|\mathcal{U}|, |\mathcal{S}|)$. We create a $n \times n$ grid G_n . Let $\mathcal{C}(G_n)$ be the set of masks of G_n . We construct a scoring function μ as follows: Let M be a mask. Let $I = \{i | (i, 0) \in M\}$, and $S_I = \{S_j | j \in I \wedge S_j \in \mathcal{S}_I\}$. $\mu(M) = 1$ if and only if the following condition holds (otherwise $\mu(M) = 0$): $|I| \leq k$ and $\cup_{j \in I} S_j = \mathcal{U}$. It is easy to see that $MASK_P(n, \mu, n^2, 1)$ has a satisfying solution iff the instance of the set cover problem has a solution. This proves that the problem is NP-hard. Given a solution to the problem $MASK_P(n, \mu, r, t)$, it is easy to check that it is a valid solution in polynomial time, so the problem is NP. Therefore, $MASK_P(n, \mu, r, t)$ is NP-complete. \square

D Experiment Details and Hyper-parameters

Hyper-parameters. We set $\beta = 1$, $\eta = 500$, and the query budget b to 20k. In both approaches, we test over $n = 100$ transformations and take $q = 10$ gradient samples. Once we have a final attack, we re-evaluate the survivability over $n = 1000$ transforms to get a better estimate of how well it will perform. In practice, the difference between survivability on 100 vs. 1000 transformations was often within 3%.

For transformations, we model rotation about the y axis with homography matrices, lighting changes with gamma correction, and focus changes with Gaussian blurring. For our GTSRB [36] attack we set rotation about the y axis to be between -50° and 50° and fix the base focal length $f = 3$ ft. The projected image plane distance is allowed to vary between f and 15 ft. Crop sizes and offsets can vary between 0% and 3.125%. The max γ effect can be 3.5 for

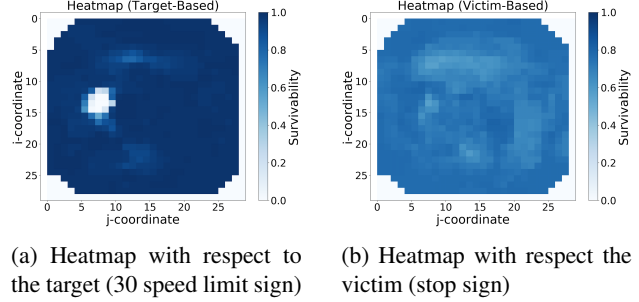


Figure 5: Example heatmaps.

darkening (or $\frac{1}{3.5}$ for lightening), and use Gaussian kernels of size 1, 5, and 9. All parameters are sampled uniformly.

For our ALPR attack, we set rotation to be between -15° and 15° and fix the base focal length $f = 10$ ft. We set the Gaussian kernels to sizes 1, 3, and 5, and let the remaining parameters match the GTSRB attack.

E Additional Results

This section includes additional analysis on heatmap estimation, digital survivability results, and an ablation study of mask reduction techniques.

Heatmap Estimation In general, the heatmap is a function of the point at which it is estimated. The heatmap can also be computed relative to the target (as is done in our algorithm as described in Section 4.1.1) or relative to the victim. For a Stop sign to Speed limit 30 km / hr attack, a relative to target heatmap overlaps a 30 over the Stop sign and sees the survivability drop by removing one patch of the 30 at a time. A relative to victim heatmap would take the Stop sign and try adding one patch of the 30 at a time. Fig. 5a shows the heatmap with respect to the target and Fig. 5b shows the heatmap relative to the victim. We found the victim heatmap to be ineffective because the survivability of the target label tended to remain 0.

In principle, the heatmap could be measured at multiple points during the algorithm, but the measurement is expensive in terms of number of queries and computation time. Empirically, we found that just using one heatmap (in our case, the target one) worked well in practice. The white area in Fig. 5a is interesting – it suggests that area is likely to be crucial for applying a patch in order to convert the stop sign to the speed limit 30 km/hr sign. Conversely, darker areas in Fig. 5a are good candidates for elimination from the mask.

Digital Survivability Results In Table 6 we provide the images generated for the attacks listed in Table 1 alongside with the survivability, mask pixel, and mask to object size

Table 6: Sample of digital targeted attacks on GTSRB-Net. Ran with $s_{lo} = 70\%$, $s_{hi} = 90\%$, $n = 100$ during attack. Final survivability calculated on $n = 1000$ transformations.

		Target				
						
Victim						
						
<i>Final Survivability</i>		79%	78.7%	84.3%	90%	
<i>Mask Pixels</i>		35	75	55	70	
<i>Mask to Object Size Ratio</i>		4.99%	10.68%	7.83%	9.97%	
						
<i>Survivability</i>		98.1%	95.4%	97.1%	100%	
<i>Mask Bits</i>		15	143	63	0	
<i>Mask to Object Size Ratio</i>		2.26%	21.54%	9.49%	0%	

ratio statistics. Table 6 shows qualitatively that GRAPHITE attacks tend to find small regions to perturb in order to attack the classifier.

Ablative Study of Mask Reduction We present an ablative study over different reduction strategies in mask generation to enforce a specific minimum survivability threshold. The results are shown in Table 7. For these results we attack a Stop sign to become a speed limit 30 km/hr sign under three settings: the full mask generation pipeline as described in Section 4.1, only reducing the mask in a coarse-grained manner, and only reducing the mask in a fine-grained manner. The minimum threshold is 70%.

These results show that both reduction processes have benefit. While using only fine-grained reduction yields similar survivability and mask size results to the full algorithm, it uses almost 10k more queries and takes some more time. When only using coarse grained reduction, many more pixels are included to reach the same minimum 70% threshold, and thus these masks are much larger.

F Discussion and Limitations

We found that good thresholds s_{lo} and s_{hi} can be different across varied attack pairs. This means that for optimal results some tuning of these parameters could be required. As an example, the 30 km/hr to yield to passenger (Table 6) patch has 143 bits and 95.4% digital survivability. Changing s_{lo} to 0.5 results in a smaller 114-pixel perturbation with 94% survivability. This is not entirely unexpected since this is a joint-optimization problem and multiple solutions will exist depend on the weights assigned to different objectives.

One limitation in our work is that our transformations currently simulate viewpoint changes to 2D objects such as flat traffic signs (see Section A for description of our transformation models). GRAPHITE’s approach is however agnostic to the transforms model. Fundamentally, we just require access to a set of transforms from which we can sample to estimate survivability. Furthermore, the transforms do not have to be differentiable, because we are in the hard-label setting.

One limitation in hard-label attacks is that the starting point has to be a viable solution. Else, there is a risk of getting stuck in a valley with no viable solutions nearby to allow climbing out of the valley. In an earlier version of

Table 7: Ablative study of reduction types. We present final survivability and pixel counts. Attack is stop sign to speed limit 30 km/hr. Full algorithm uses $s_{lo} = 70\%$ and $s_{hi} = 90\%$, only fine reduction uses $s_{lo} = 70\%$, and only coarse reduction uses $s_{hi} = 70\%$

	Final survivability $n = 1000$	Final number of pixels	Queries	Run time
Only Fine Reduction	89.3%	68	131.9k	541.6s
Only Coarse Reduction	89.6%	159	96.0k	397.3s
Full Algorithm	90%	70	123.7k	518.7s

GRAPHITE, we did not have an automatic mask generation algorithm and were crafting candidate masks by hand. We often ran into situations where patches based on our hand-crafted mask had zero survivability and failed to successfully boost. We found that GRAPHITE significantly alleviates this problem since it starts with a large patch, which is usually survivable, and then reduces and boosts it.